International Journal of Nanomedicine

Dovepress
open access to scientific and medical research

Open Access Full Text Article

ORIGINAL RESEARCH

Preparation of Apoptotic Extracellular Vesicles from Adipose Tissue and Their Efficacy in Promoting High-Quality Skin Wound Healing

Jia Dong[1], Bin Wu[1], Weidong Tian[2,3]

[1]Department of Stomatology, People's Hospital of Longhua Shenzhen, Shenzhen, Guangdong, People's Republic of China; [2]State Key Laboratory of Oral Disease, Engineering Research Center of Oral Translational Medicine, Ministry of Education, West China School of Stomatology, Sichuan University, Chengdu, Sichuan, People's Republic of China; [3]National Engineering Laboratory for Oral Regenerative Medicine, Sichuan University, Chengdu, Sichuan, People's Republic of China

Correspondence: Jia Dong; Weidong Tian, Email scu2013dongjia@sina.com; drtwd@sina.com

Purpose: A lot of strategies have been attempted to achieve high-quality skin wound healing, among them, fat transplantation has been used for skin wound repair and scar management and has shown beneficial effects. However, the underlying mechanism is still unclear. Recently, studies found that transplanted cells underwent apoptosis within a short period and apoptotic extracellular vesicles (ApoEVs) might play the therapeutic role.

Methods: In this study, we directly isolated apoptotic extracellular vesicles from adipose tissue (ApoEVs-AT) and evaluated their characteristics. In vivo, we investigated the therapeutic role of ApoEVs-AT in full-thickness skin wounds. The rate of wound healing, the quality of granulation tissue, and the area of scars were evaluated here. In vitro, we investigated the cellular behaviors of fibroblasts and endothelial cells induced by ApoEVs-AT, including cellular uptake, proliferation, migration, and differentiation.

Results: ApoEVs-AT could be successfully isolated from adipose tissue and possessed the basic characteristics of ApoEVs. In vivo, ApoEVs-AT could accelerate skin wound healing, improve the quality of granulation tissue, and reduce the area of scars. In vitro, ApoEVs-AT could be engulfed by fibroblasts and endothelial cells, significantly enhancing their proliferation and migration. Moreover, ApoEVs-AT could promote adipogenic differentiation and inhibit the fibrogenic differentiation of fibroblasts.

Conclusion: These findings indicated that ApoEVs could be successfully prepared from adipose tissue and showed the ability to promote high-quality skin wound healing by modulating fibroblasts and endothelial cells.

Keywords: apoptotic extracellular vesicles, adipose tissue, skin wound healing, fibroblasts, endothelial cells

Introduction

The skin played a major role in interfacing between the external environment and the human body, so it always suffered a variety of injuries.[1] Studies showed that the healing of skin injuries followed four overlapping steps: hemostasis, inflammation, proliferation, and remodeling,[2,3] and these steps were adjustable As dermal adipose tissue was an important contributor to skin development and regeneration, transplantation of adipose tissue or its components was considered a high-potential therapeutic strategy.[4] Several studies have applied adipose tissue for treating skin wounds and scars and have achieved excellent therapeutic effects. However, the underlying mechanism was not fully understood. The theory that transplanted live cells released growth factors, cytokines, and extracellular vesicles (such as exosomes) through the paracrine pathway to exert therapeutic effects has been widely recognized. However, recent studies found that transplanted cells underwent extensive apoptosis in a short time.[5–7] Therefore, they suggested that the process of apoptosis might take a large part in the therapeutic abilities of transplanted cells.

Apoptosis, the process of programmed cell death, first reported in 1972 by Kerr et al[8] played an important role in inflammation resolution, tissue homeostasis maintenance, pathogenesis, development, and aging.[8,9] Apoptotic cells could release a great number of extracellular vesicles, which were identified as apoptotic extracellular vesicles (ApoEVs).[10]

Received: 22 March 2023
Accepted: 30 May 2023
Published: 2 June 2023

Traditionally, Apoptotic bodies (ApoBDs, 1–5 μm) were the only known population. In recent years, ApoEVs isolated by gradient centrifugation mainly contained smaller extracellular vesicles (< 1 μm), which were also considered an exosome-like subpopulation. Nanometer-sized vesicles were more conducive to various applications. Some studies have reported that ApoEVs could be isolated from MSCs, including bone marrow mesenchymal stem cells (BMSCs),[11–17] adipose mesenchymal stem cells (ASCs),[14] umbilical cord mesenchymal stem cells (UMSCs),[18] and deciduous pulp stem cells,[19] etc. However, whether ApoEVs could be isolated directly from whole tissue was unknown.

MSCs-derived ApoEVs showed a therapeutic effect in various diseases, like bone repair,[12] oral disease,[11,19] endocrine disease,[17] etc. As for the relationship between ApoEVs and skin tissue, only a few studies have been reported. Qu et al found that human embryonic stem cells (ESCs)-derived ApoEVs inherited pluripotent-specific molecules SOX2 from ESCs. They also found that ESCs-derived ApoEVs could accelerate skin wound healing via transferring SOX2 into skin MSCs via activating the Hippo signaling pathway.[18] Ma et al found that epithelial stem cells (EPCs)-derived ApoEVs could maintain the number of stem cells and the homeostasis of epithelial tissue in the skin. Besides, they found that exogenous ApoEVs promoted wound healing and hair growth via activating the Wnt/β-catenin pathway in skin and hair follicle mesenchymal stem cells.[15] Therefore, based on previous reports on the relationship between adipose tissue and skin, as well as the functionality of ApoEVs, we speculated that adipose tissue-derived ApoEVs might promote skin wound healing and scar remodeling.

In this study, we first assumed that ApoEVs could be prepared directly from adipose tissue and they would promote high-quality skin wound healing. To verify this assumption, we improved the method of preparing ApoEVs from MSCs to successfully isolate ApoEVs-AT from whole adipose tissue and identified their characteristics. Then, we treated full-thickness skin wounds with ApoEVs-AT to investigate the ability to promote skin wound healing and reduce scar formation. In addition, we also evaluated the effect of ApoEVs-AT on the behaviors of fibroblasts and endothelial cells.

Materials and Methods

Animals

Sprague Dawley (SD) rats were purchased from Chengdu Dashuo experimental animal Co., Ltd (China). All operations of animals were reviewed and approved by the Ethics Committees of the State Key Laboratory of Oral Diseases, West China School of Stomatology, Sichuan University (approval number: WCHSIRB-D-2023-218). All animal experiments were performed according to protocols approved by the Institutional Animal Care and Use Committee (IACUC) at Sichuan University and followed the Animal Research: Reporting of in Vivo Experiments (ARRIVE) guidelines.

Preparation of ApoEVs-AT

Inguinal adipose tissue was isolated from 4-week-old SD rats, cut into small pieces (1–2 cm^3), and transferred into a suspension culture flask (Wheaton, USA). Serum-free minimum essential medium α (α-MEM, HyClone, USA) with 250 nM staurosporine (STS, Beyotime, China) was added to the flask. The mixture was cultured in a 5% CO_2-95% air atmospheric condition at 37°C with speed at 200 rpm for 2 days. Tissue pieces were removed by gauze and the supernatant was collected. The debris of tissues and larger extracellular vesicles were removed by centrifugation at 800 g for 10 min at 4°C and 2000 g for 15 min at 4°C. The supernatant was further collected and centrifuged at 16,000 g for 30 min at 4°C to obtain ApoEVs-AT. ApoEVs-AT were suspended in PBS for further testing.

Characterization of Native and Apoptotic Adipose Tissue

Native adipose tissue and apoptotic adipose tissue were harvested, fixed in 4% neutral paraformaldehyde (Biosharp, USA), dehydrated in gradient ethanol, transparent in xylene, and finally embedded in paraffin and cut into 5–6 μm thick sections. The morphology was detected by H&E staining (Solarbio, China) according to the manufacturer's protocol. The apoptosis of adipose tissue was evaluated by TdT-mediated dUTP nick-end labeling (TUNEL) assay, which was usually used for apoptosis detection.[17] According to the manufacturer's instruction of the TUNEL Apoptosis Assay Kit (Beyotime, China), sections were incubated with TUNEL reagent at 37°C for 60 min. Then, DAPI (1:1000, Solarbio, C0050) was used to further mark the nuclei at room temperature for 5 min. Images were captured by confocal microscopy (Olympus FV1000, Japan).

Characterization of ApoEVs-AT

The protein concentration of ApoEVs-AT was measured by the BCA protein assay kit (KeyGEN BioTECH, China) using the manufacturer's protocol. The size distribution was measured by the ZetaView analysis system (Particle Metrix, Germany). For morphology observation, ApoEVs-AT were loaded onto formvar carbon-coated grids, negatively stained with aqueous phosphotungstic acid at room temperature for 60 s, and imaged by transmission electron microscope (TEM, Tecnai G2 F20 S-Twin, USA). For phosphatidylserine (PtdSer) detection, ApoEVs-AT were suspended in 100 μL PBS and 5 μL FITC Annexin V (BD, USA) was added to incubate at room temperature for 15 min. Images were captured by confocal microscopy (Olympus FV1000, Japan). The apoptosis-specific marker proteins were detected by Western blot. Briefly, 50 μg ApoEVs-AT were mixed with 4×loading buffer (Solarbio, China) and boiled for 10 min. Proteins were resolved on 10% or 15% SDS-PAGE gel electrophoresis (120 V, 90 min) and blotted onto a nitrocellulose membrane. Then, the membrane was incubated with primary antibodies, cleaved caspase-3 (1:1000, Cell Signaling Technology, #9664), caveolin-1 (1:1000, Sangon Biotech, D161423), RhoA (1:1000, Abcam, ab187027), Histone H3 (1:1000, Invitrogen, PA5-16,183), perilipin A (1:1000, Abcam, ab3526), and actin (1:1000, Abcam, ab179467) at 4°C overnight. Horseradish peroxidase (HRP) conjugated secondary antibodies were followed to incubate at room temperature for 2 h. High sig ECL Western Blotting Substrate (Tanon, China) was used for detecting protein signals by ImageQuant LAS 4000 mini machine (GE Healthcare, USA).

Animal Experiments

All operations were performed on 4-week-old male SD rats (75 ± 10 g, n=6) under general anesthesia with 1% pentobarbital sodium (10 mL/kg, intraperitoneal injection). The dorsal area was shaved and sterilized with 75% ethanol. Two circular full-thickness skin wounds (2 cm in diameter) were prepared by resecting according to the circle marked with a pen. The wounds were divided into two groups: the blank group (left) and the ApoEVs-AT group (right). In the blank group, 100 μL PBS was subcutaneously injected around the wounds at 4 points. In the ApoEVs-AT group, 100 μL PBS containing 200 μg ApoEVs-AT also was subcutaneously injected around the wounds at 4 points. To ensure the therapeutic effect of ApoEVs-AT, injections in each group were performed every 4 days. Digital photographs were taken on days 0, 4, 8, 12, 16, and 40. The wound area was measured using the ImageJ 1.53a software. Rats were euthanized on day 8 and day 40 respectively (n=3 per timepoint), via rapid cervical dislocation, and the samples were harvested for further testing.

Hematoxylin and Eosin (H&E) Staining and Masson Staining

To conduct histological evaluation, the harvested samples were fixed overnight in 4% neutral paraformaldehyde (Biosharp, USA), dehydrated in gradient ethanol, transparent in xylene, and finally embedded in paraffin and cut into 5–6 μ m thick sections. The sections near the center of the wound were used for further testing. H&E staining (Solarbio, China) was performed to visualize the structure of wounds and scars. Masson staining (Baso, China) was performed to visualize the collagen fibers according to the manufacturer's instructions.

Immunofluorescence Staining

To further evaluate the specific structure of the samples, the sections near the center of the wound were blocked with 5% bovine serum albumin (BSA, Sigma-Aldrich, USA) at room temperature for 2 h and then incubated with primary antibodies at 4°C overnight. Primary antibodies, CD31 (1:200, Abcam, ab24590) and perilipin A (1:200, Abcam, ab3526), were used to mark blood vessels and adipocytes, respectively. Primary antibodies, alpha-smooth muscle actin (α-SMA, 1:200, Abcam, ab5694), collagen 1(Col 1, 1:200, Abcam, ab270993), and collagen 3 (Col 3, 1:200, Abcam, ab184993), were used to mark different types of fibers. Next, the secondary antibodies, goat anti-mouse 488 (1:200, Invitrogen, A11008) and goat anti-rabbit 555 (1:200, Invitrogen, A21428), were followed to incubate at 37°C for 1 h. Lastly, DAPI (1:1000, Solarbio, C0050) was used to mark the nuclei at room temperature for 5 min. Images were captured by confocal microscopy (Olympus FV1000, Japan) and analyzed by the ImageJ 1.53a software (n=3).

Cell Culture

Fibroblasts (HFF cell line) and endothelial cells (HUVEC cell line) were purchased from the Cell Bank of the Chinese Academy of Sciences (China). These cells were seeded in minimum essential medium α (α-MEM, HyClone, USA) supplemented with 10% fetal bovine serum (FBS, Gibco, USA), 100 U/mL penicillin, and 100 g/mL streptomycin, and cultured in a 5% CO_2-95% air atmospheric condition at 37°C. When cells reached 85–95% confluence, they were trypsinized and passaged at a 1:2 ratio.

Cellular Uptake

For cellular uptake, 5×10^4 HFFs or HUVECs were first seeded into a confocal culture dish (NEST, China). Then, 100 μg ApoEVs -AT, suspended in 1 mL α-MEM, were labeled with 1 μg membrane-labeling dye DiO (Life Tech, V22886) at 37°C for 30 min, re-purified with the centrifugation at 16,000 g for 30 min at 4°C. HFFs or HUVECs were cultured with DiO-labeled ApoEVs-AT for 0, 4, and 8 h. Cells were fixed in 4% neutral paraformaldehyde (Biosharp, USA) at room temperature for 10 min and underwent permeabilization with 0.05% Triton X-100 (Sigma-Aldrich, USA) at room temperature for 15 min. The cytoskeleton was stained with phalloidin (1:200, Invitrogen, A34055-300U) at room temperature for 20 min and the nuclei were stained with DAPI (1:1000, Solarbio, C0050) at room temperature for 5 min. Images were captured by confocal microscopy (Olympus FV1000, Japan).

CCK-8 Assays

To investigate the proliferative activity of cells, CCK8 assays were usually chosen.[20] HFFs or HUVECs were seeded at 2×10^3 cells per well into a 96-well plate. Cells were divided into the blank group (100 μL PBS per well) and the ApoEVs-AT group (100 μL PBS containing 5 μg ApoEVs-AT per well). The culture medium per well was changed every 2 days to maintain the treatment effect. After 2, 4, 6, 8, and 10 days of culture, the proliferative activity was tested according to the Cell Counting Kit-8 (CCK-8, KeyGEN BioTECH, China) procedure. Briefly, 10 μL CCK8 solution was added to each well and cultured at 37°C for 1 h. Then, the optical density (OD) value was measured at a wavelength of 450 nm and used to produce CCK-8 growing curves (n=3).

Scratch Assays

To investigate the migration ability of fibroblasts, HFFs were seeded at 1×10^5 cells per well into a 24-well plate. When cells contacted and formed a confluent monolayer, pipette tips were used to scratch according to the marked line. Images at this time (0 h) were captured by an inverted microscope (Olympus, Japan). Then, cells were divided into the blank group (500 μL PBS per well) and the ApoEVs-AT group (500 μL PBS containing 25 μg ApoEVs-AT per well). After culturing for 16 h, Images were captured again by an inverted microscope (Olympus, Japan). The migrated area was measured using ImageJ 1.53a software (n=3).

Transwell Assays

Transwell assays were also used to analyze the migration ability of cells. HFFs or HUVECs were seeded at 1.5×10^4 cells per well into the upper chamber of a Transwell (Corning, USA). Cells were divided into the blank group and the ApoEVs-AT group. In the blank group, 500 μL PBS was added to the lower chamber. In the ApoEVs-AT group, 500 μL PBS containing 25 μg ApoEVs-AT was added to the lower chamber as a chemoattractant. After culturing for 12 h, nonmigratory cells in the upper chamber were removed. The migrated cells were fixed with 4% neutral paraformaldehyde (Biosharp, USA) at room temperature for 10 min and stained with 0.1% crystal violet (Sigma-Aldrich, USA) at room temperature for 15 min. Images were captured by an inverted microscope (Olympus, Japan) and the number of migrated cells was measured using ImageJ 1.53a software (n=3).

Quantitative Real-Time Polymerase Chain Reaction (qRT-PCR)

To investigate the differentiation of fibroblasts induced by ApoEVs-AT, HFFs were seeded at 1×10^5 cells per well into a 24-well plate. Cells were divided into the blank group (500 μL PBS per well) and the ApoEVs-AT group (500 μL PBS containing 25 μg ApoEVs-AT per well). The culture medium per well was changed every 2 days to maintain the treatment effect. After 20 days of culture, cells were collected. The RNAiso Plus (TaKaRa Biotechnology, Japan) was used to extract total RNA, which was reverse transcribed into cDNAs using the RevertAid First Strand cDNA Synthesis Kit (Thermo Scientific, USA). The synthesized cDNAs were amplified with SYBR Premix ExTaq (TaKaRa Biotechnology, Japan) using QuantStudio 6 Flex Real-Time PCR System (Life Technologies, China). The PCR cycling parameters were at 95 °C for 2 min, 44 cycles at 95 °C for 5 s, and at 60 °C for 30s. Primer sequences were listed in Supplementary Table S1 (n=3).

Tube Formation Assays

To investigate the angiogenesis of endothelial cells induced by ApoEVs-AT, HUVECs were divided into the blank group and the ApoEVs-AT group. In the blank group, cells were cultured in the normal culture medium. In the ApoEVs-AT group, cells were pretreated with 50 μg/mL ApoEVs-AT overnight. Then, cells were collected, and seeded at 1×10^4 cells per well into a 96-well plate, which was coated with 50 μL Matrigel (Corning, USA). After culturing for 5 h, images were captured by an inverted microscope (Olympus, Japan). The number of nodes, number of meshes, and total length were analyzed by ImageJ 1.53a software (n=3).

Statistical Analysis

All statistical analyses were performed using Microsoft Excel or GraphPad Prism 7 software. All results were expressed as mean value ± standard deviation. An unpaired two-tailed Student's *t*-test was used to determine the level of significance. $*p < 0.05$, $**p < 0.01$, $***p < 0.001$, $****p < 0.0001$.

Results

Preparation and Characterization of ApoEVs-AT

First, adipose tissue (AT) was isolated, cut into small pieces, and transferred into a suspension culture flask. Then, α- MEM and staurosporine (STS) were added to the flask. The mixture was cultured for 2 days to induce apoptosis of adipose tissue. Then, ApoEVs-AT were isolated from the supernatant by gradient centrifugation as described by Zhang et al[14] (Figure 1A). The structure and apoptosis of adipose tissue were evaluated by H&E and TUNEL staining, respectively. Compared with native adipose tissue, apoptotic adipose tissue was structurally loose and irregular (Figure 1B). TUNEL-stained images demonstrated apoptosis occurred in many cells of apoptotic adipose tissue, in contrast, no TUNEL-stained nuclei appeared in native adipose tissue (Figure 1C). To further evaluate the characteristics of ApoEVs-AT, the morphology, size distribution, and specific markers were analyzed. By transmission electron microscopy (TEM) analysis, ApoEVs-AT showed a typical double-membrane spherical structure (Figure 1D). By nanoparticle tracking analysis (NTA), most ApoEVs-AT ranged from 25 to 400 nm and the average size was 155.4 nm (Figure 1E). Immunofluorescence images indicated that ApoEVs-AT were positive for the apoptosis-specific marker, phosphatidylserine (PtdSer),[17] which was presented by Annexin V staining (Figure 1F). Western blot analysis indicated that ApoEVs-AT expressed apoptosis-specific marker proteins,[14] cleaved caspase-3, caveolin-1 (Cav-1), RhoA, and histone H3, and adipocyte-specific marker protein, perilipin A. The cytoskeleton protein, actin, was also slightly expressed in ApoEVs-AT (Figure 1G). These results suggested that ApoEVs could be successfully prepared from adipose tissue after culturing with STS for 2 days and the characteristics of ApoEVs-AT identified their high purity.

ApoEVs-AT Accelerated Full-Thickness Skin Wound Healing

To evaluate the effect of ApoEVs-AT in promoting full-thickness skin wound healing, two full-thickness skin wounds (2 cm in diameter) were established on the dorsum of each SD rat. In the blank group (left), 100 μL PBS was subcutaneously injected around the wounds every 4 days as a control to support comparison. In the ApoEVs-AT group (right), 100 μL PBS containing 200 μg ApoEVs-AT also was subcutaneously injected around the wounds every 4 days (Figure 2A). Digital photographs were taken on day 0, day 4, day 8, day 12, and day 16 to measure the rate of

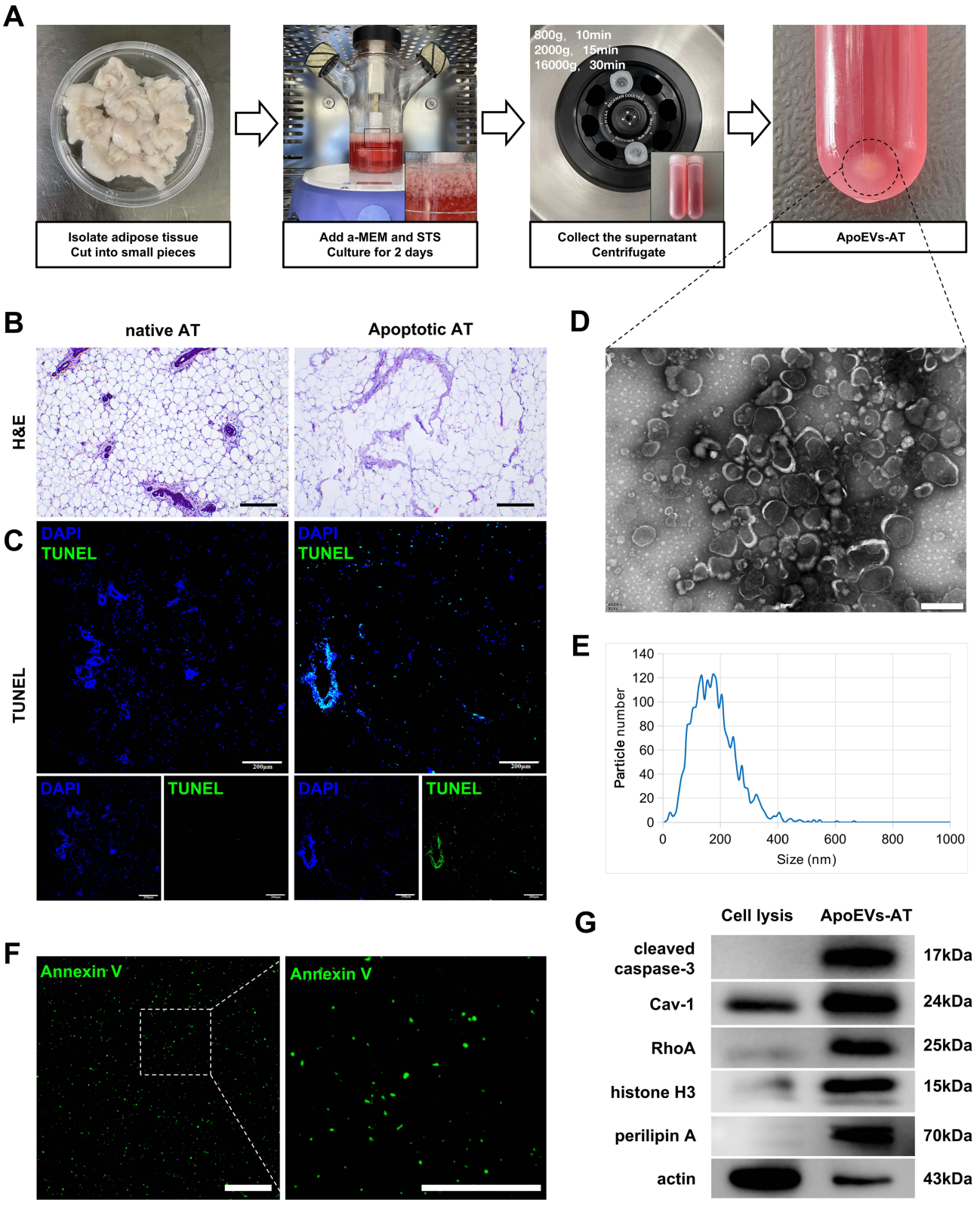

Figure 1 Preparation and characterization of ApoEVs-AT. (**A**) Schematic view of the process of preparing ApoEVs-AT from adipose tissue. (**B**) Representative images of native adipose tissue and apoptotic adipose tissue with H&E staining. (Scale bar = 200 μm.) (**C**) Representative images of native adipose tissue and apoptotic adipose tissue with TUNEL staining. (Green: TUNEL-stained apoptotic cells; Blue: DAPI-stained nuclei. Scale bar = 200 μm.) (**D**) Representative images of ApoEVs-AT with transmission electron microscopy. (Scale bar = 500 nm.) (**E**) The size distribution of ApoEVs-AT was measured by nanoparticle tracking analysis. (**F**) Representative images of ApoEVs-AT with Annexin V staining. The white dotted box represented the area that was magnified in the right-magnified panel. (Green: Annexin V-stained ApoEVs-AT. Scale bar = 10 μm.) (**G**) Western blot analysis of marker proteins, cleaved caspase-3, caveolin-1 (Cav-1), RhoA, histone H3, perilipin A, and actin.

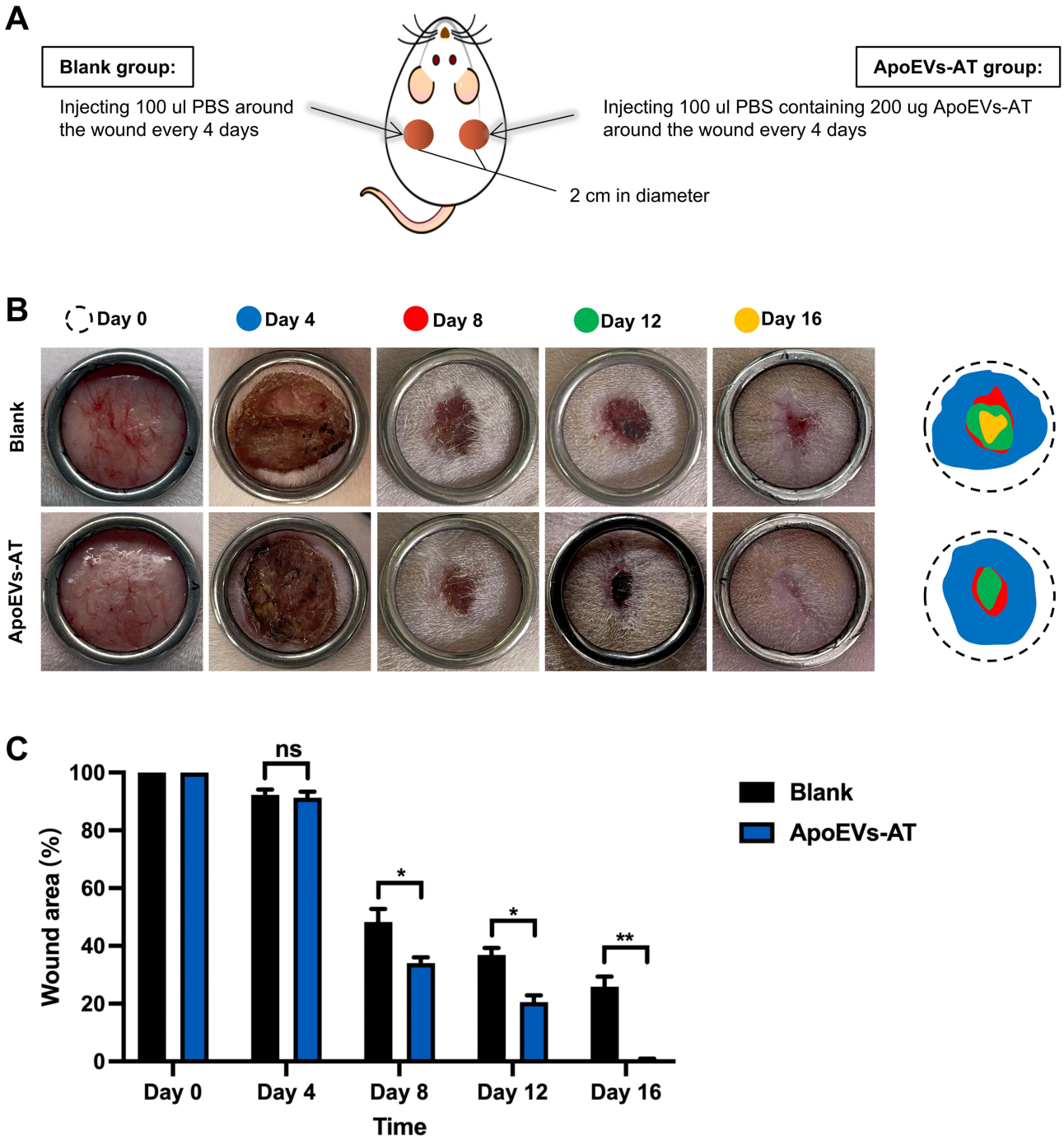

Figure 2 Skin wound healing was accelerated by ApoEVs-AT. (**A**) Schematic view of the experimental operation process. (**B**) Representative digital photographs of wound areas on day 0, day 4, day 8, day 12, and day 16. Pattern graphs of wound areas were established for each time point. The dotted circles pointed out the initial wounds, and the colored parts pointed out the wound areas at different time points. (Diameter of the ring = 2 cm.) (**C**) The area of unhealed wounds was analyzed (n=3). Wound area (%) was defined as: unhealed wound area at day X / initial wound area at day 0×100%. The significance was tested with an unpaired two-tailed Student's *t*-test. ($^{ns}p>0.05$, $^{*}p<0.05$, $^{**}p<0.01$).

healing. Pattern graphs were established to indicate the edge of wounds more clearly. The dotted circle represented the edge of initial wounds at day 0 and the colored part represented the area of unhealed wounds at different time points (Figure 2B). Wound area (%) was defined as: unhealed wound area at day X / initial wound area at day 0×100%. After statistics, we found that ApoEVs-AT showed the ability to accelerate wound healing after twice of injections (day 0 and day 4), based on the results on day 8 that adding ApoEVs-AT reduced the average wound area from 48.27% (the blank group) to 34.03% (the ApoEVs-AT group) (Figure 2C). Similarly, after 3 times of injections (day 0, day 4, and day 8), adding ApoEVs-AT reduced the average wound area from 36.87% (the blank group) to 20.57% (the ApoEVs-

AT group) on day 12 (Figure 2C). Further, after 4 times of injections (day 0, day 4, day 8, and day 12), all full-thickness skin wounds healed in the ApoEVs-AT group on day 16, in contrast, the average wound area on day 16 in the blank group was 25.87%, significantly different from that of the ApoEVs-AT group (Figure 2C). These results suggested that ApoEVs-AT were able to accelerate full-thickness skin wound healing.

ApoEVs-AT Improved the Quality of Granulation Tissue

In addition to the rate, the quality of healing was another issue that researchers focused on. The regeneration of skin structure was optimal, but most wounds were eventually replaced by scars. To evaluate the quality of skin wound healing, we first evaluated the quality of unhealed wounds (granulation tissue), which would greatly affect the quality of healed skin. Skin wounds on day 8 were collected and sections were made for subsequent staining. By H&E staining, the rate of re-epithelization was accelerated by ApoEVs-AT, based on the results that the area without epithelization was narrower in the ApoEVs-AT group than that in the blank group (Figure 3A), which was consistent with the results of digital photographs (Figure 2B and C). Therefore, the statistical analysis of the re-epithelization length was omitted here. By H&E staining and Masson staining, wounds were mainly connected by granulation tissue and covered with a scab shell. In the ApoEVs-AT group, the granulation tissue was thicker, and the composition was more diversified than that of the blank group (Figure 3B). The average thickness of granulation tissue in the ApoEVs-AT group was 1342.26 μm. However, the average thickness in the blank group was 826.32 μm, and the difference was statistically significant (Figure 3C). By Masson staining, we found that collagen fiber was the main component of granulation tissue both in the ApoEVs-AT group and in the blank group, but there were more blood vessels in the ApoEVs-AT group, which was further confirmed by immunofluorescence staining of CD31, a universal marker of endothelial cells (Figure 3D). Besides, the number of blood vessels in the ApoEVs-AT group was statistically different from that in the blank group (Figure 3E). Moreover, previous studies have reported that adipocytes were extremely important in skin development and regeneration.[21,22] Interestingly, adipocytes appeared in each wound of the ApoEVs-AT group, which were stained by perilipin A, in contrast, nearly no adipocyte appeared in the blank group (Figure 3D and F). Therefore, these results confirmed that ApoEVs-AT could improve the quality of granulation tissue during skin wound healing.

ApoEVs-AT Reduced Scar Formation

To assess the quality of healing at a later stage, we collected the healed skin on day 40 and made sections for subsequent staining. Based on the digital photographs, scar area (%) was defined as: scar area at day 40 / initial wound area at day 0×100%. After statistics, we found that the average scar area was reduced from 55.93% (the blank group) to 15.77% (the ApoEVs-AT group) by ApoEVs-AT (Figure 4A). Images with H&E staining also indicated that the scar was narrower in the ApoEVs-AT group than that in the blank group (Figure 4B). The complete epidermal structure could be found both in the ApoEVs-AT group and the blank group. However, in the ApoEVs-AT group, there were many regenerated hair follicles, which were similar to native skin. In the blank group, there was no hair follicle or other appendages (Figure 4C and D). Masson staining indicated that fibers were the main component of scars, so we further performed immunofluorescence staining on these fibers to distinguish different types. Results showed that ApoEVs-AT could reduce the expression of α-SMA, a marker of myofibroblast (Figure 4C). The relative fluorescence density (α-SMA/DAPI) was significantly reduced in the ApoEVs-AT group (Figure 4E). Besides, we also distinguished collagen 1 (Col 1) and collagen 3 (Col 3) by immunofluorescence staining and found the positive signals of Col 3 were more in the ApoEVs-AT group than that in the blank group (Figure 4C). The relative fluorescence density of Col 3/Col 1 was increased by ApoEVs-AT from 0.10 (the blank group) to 0.26 (the ApoEVs-AT group) (Figure 4F), which was related to the reduction of scar and the increase of skin softness. These results confirmed that ApoEVs-AT could promote high-quality full-thickness skin wound healing, accompanied by a decrease in scar formation and an increase in hair follicle regeneration.

ApoEVs-AT Regulated the Behavior of Fibroblasts and Endothelial Cells

To explore the cellular mechanism of ApoEVs-AT in promoting high-quality skin wound healing, we selected two types of important cells (fibroblasts and endothelial cells) in skin regeneration for in vitro experiments. After culturing fibroblasts with Dio-labeled ApoEVs-AT for 4 h, a small amount of ApoEVs-AT could be detected in fibroblasts. After extending the culture time to 8 h, the ApoEVs-AT in fibroblasts was gradually increased (Figure 5A). CCK8 assays indicated that 50 μg/mL ApoEVs-AT could considerably promote the proliferation of fibroblasts compared with the blank group (Figure 5B). The results of transwell

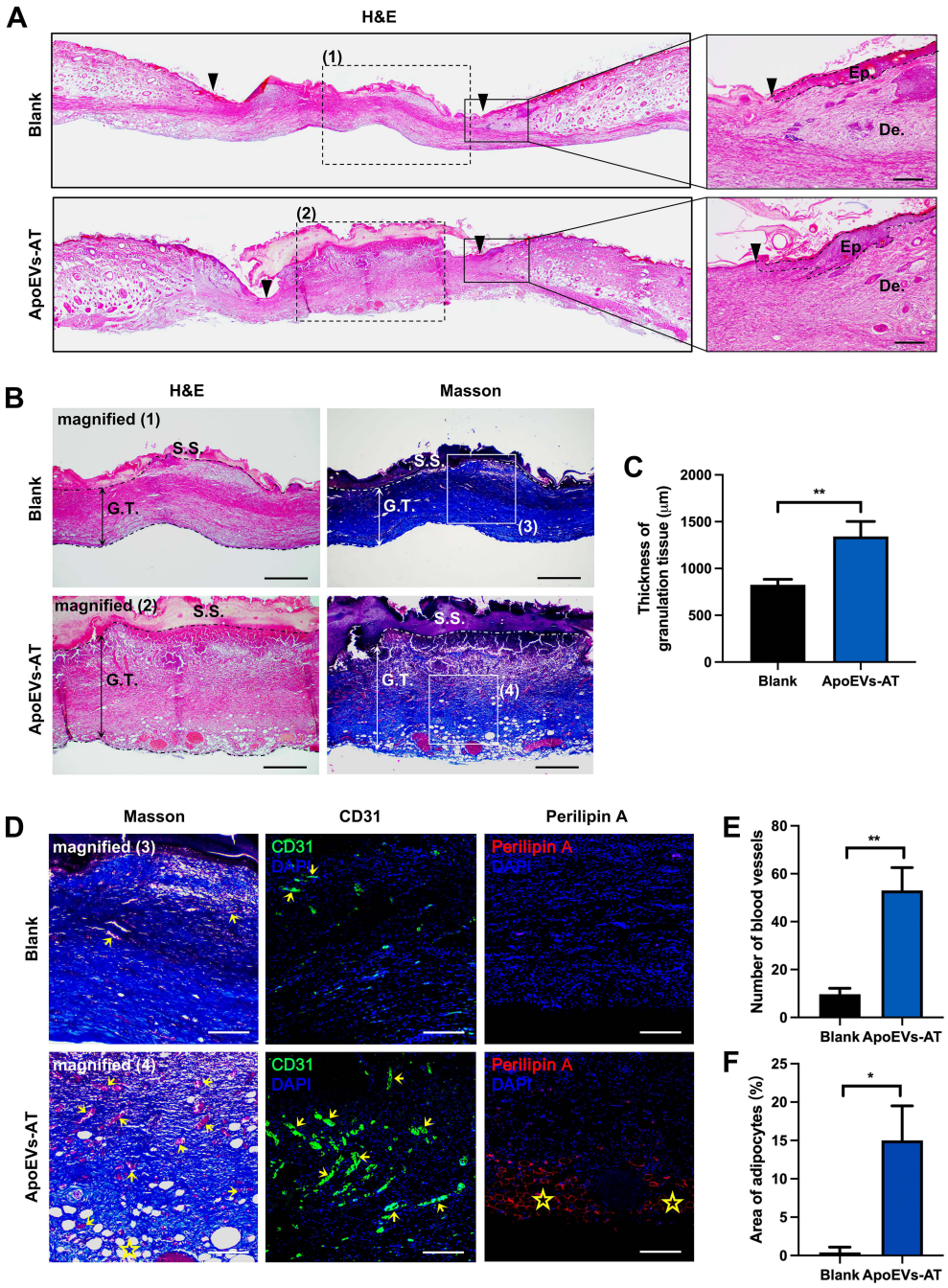

Figure 3 The quality of granulation tissue was improved by ApoEVs-AT. (**A**) Representative images of wounds on day 8 with H&E staining. The black inverted triangles pointed out the edge of the wound area/the edge of re-epithelization. The black solid boxes represented areas that were magnified. In the right magnified panels, the black dotted lines pointed out the area of the regenerated epidermis. The black dotted boxes represented areas with H&E staining that were magnified in (**B**). (Ep.: epidermis; De.: dermis. Scale bar = 200 μm.) (**B**) Representative images of granulation tissue at day 8 with H&E staining and Masson staining. The dotted lines pointed out the edge of the granulation tissue. The solid lines with double arrows represented the thickness of granulation tissue. The white solid boxes represented areas with Masson staining that were magnified in (**D**). (G.T.: granulation tissue; S.S.: scab shell. Scale bar = 500 μm). (**C**) The thickness of granulation tissue was analyzed (n=3). (**D**) Representative images of magnified areas with Masson staining and immunofluorescence staining. The yellow arrows pointed out the blood vessels. The yellow stars pointed out the area of adipocytes. (Green: CD31-stained blood vessels; Red: perilipin A-stained adipocytes, blue: DAPI-stained nuclei. Scale bar = 200 μm). (**E**) The number of blood vessels per field of view (scale bar=200 μm) was analyzed (n=3). (**F**) The area of adipocytes was analyzed (n=3). Area of adipocytes (%) was defined as: area of adipocytes/area of granulation tissue×100%. The significance was tested with an unpaired two-tailed Student's *t*-test. (*p<0.05, **p<0.01).

assays and scratch assays both showed that ApoEVs-AT could significantly promote the migration of fibroblasts (Figure 5C–F). Besides, after treating fibroblasts with ApoEVs-AT for 20 days, the expression of fibrogenic-related genes (Col 1, Col 3, and α-SMA) and adipogenic-related genes (PPARγ and C/EBPα) were evaluated by qRT-PCR. The results showed that ApoEVs-AT could reduce the expression of fibrogenic-related genes (Col 1, Col 3, and α-SMA) and increased the expression of adipogenic-

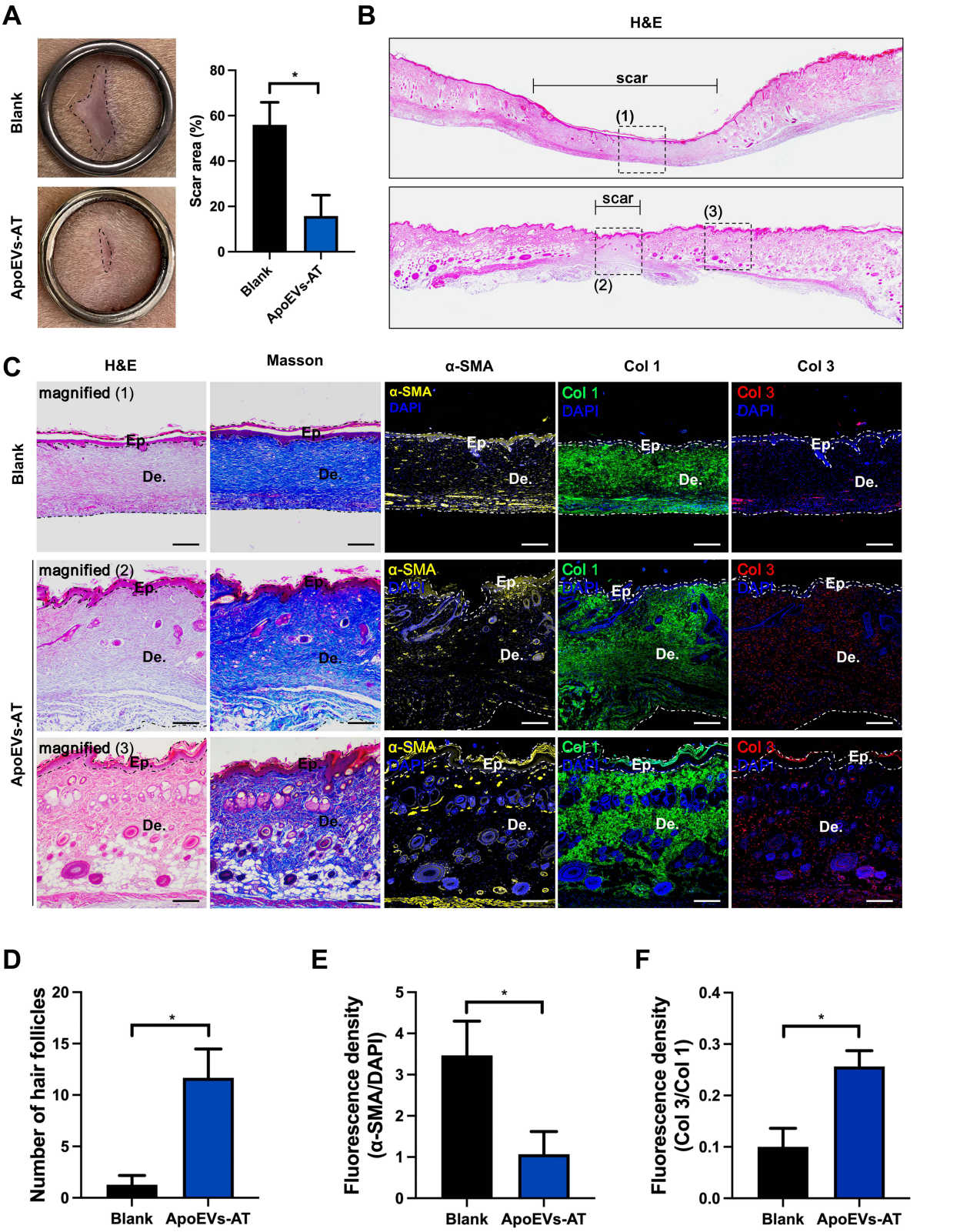

Figure 4 Scar area was reduced by ApoEVs-AT. (**A**) Representative digital photographs of scars on day 40 and the area of scars were analyzed (n=3). The black dotted lines pointed out the edge of the scars. (Diameter of the ring = 2 cm.) (**B**) Representative images of scars at day 40 with H&E staining. The black dotted boxes represented areas that were magnified in (**C**). (**C**) Representative images of magnified areas with H&E staining, Masson staining, and immunofluorescence staining. The dotted lines pointed out the edge of the epidermis and dermis. (Ep.: epidermis; De.: dermis. Yellow: α-SMA; Green: Col 1; Red: Col 3. Scale bar = 200 μm.) (**D**) The number of hair follicles per field of view (scale bar = 200 μm) was analyzed (n=3). (**E**) Relative fluorescence density (α-SMA/DAPI) per field of view (scale bar = 200 μm) was analyzed (n=3). (**F**) Relative fluorescence density (Col 3/Col 1) per field of view (scale bar = 200 μm) was analyzed (n=3). The significance was tested with an unpaired two-tailed Student's *t*-test. (*$p<0.05$).

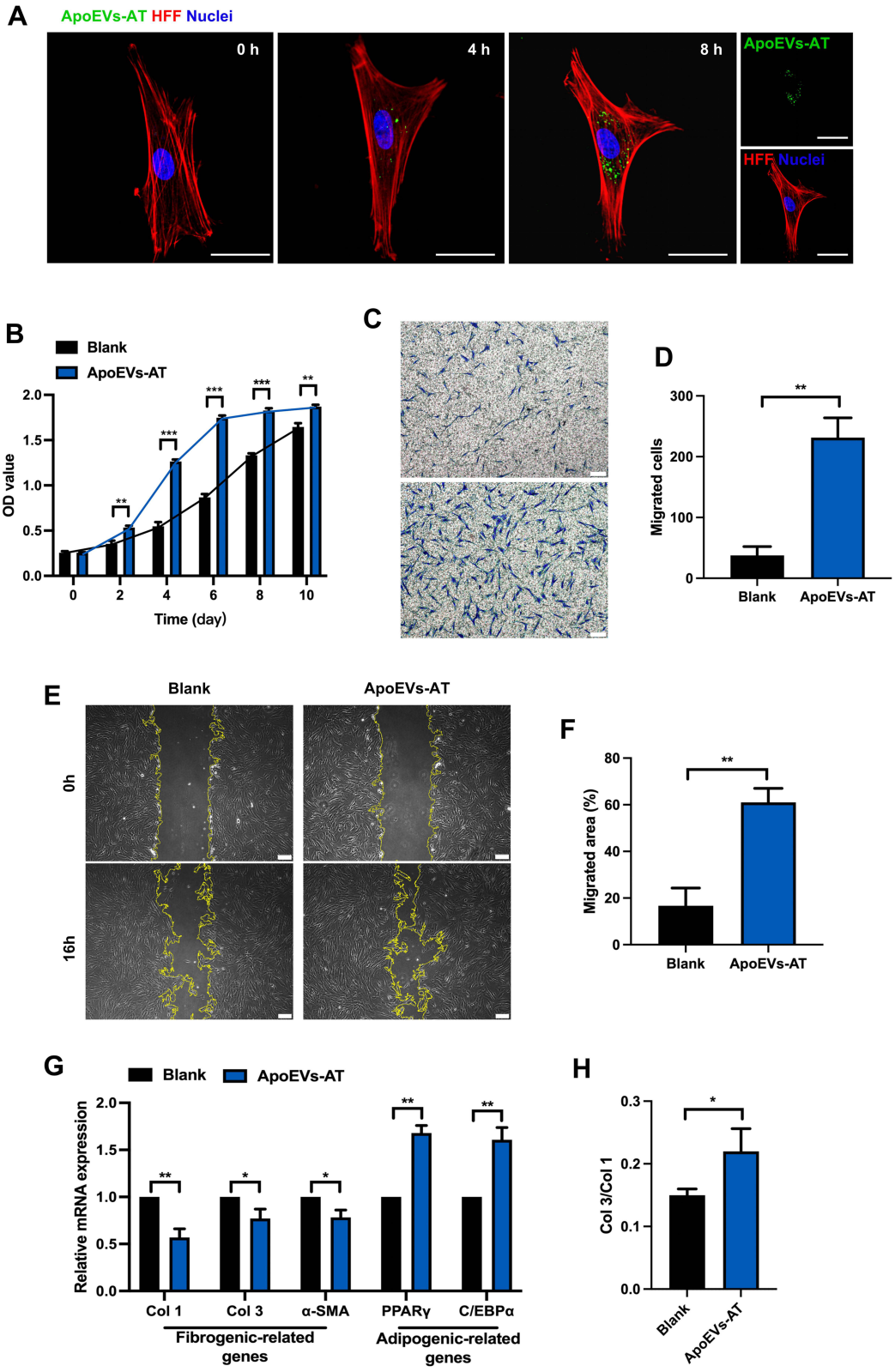

Figure 5 Behaviors of fibroblasts were regulated by ApoEVs-AT. (**A**) Uptake analysis of ApoEVs-AT by fibroblasts (Red: phalloidin-stained fibroblasts; Green: Dio-labeled ApoEVs-AT, blue: DAPI-stained nuclei. Scale bar = 40 μm.) (**B**) The proliferation of fibroblasts was measured by the CCK8 assays. (**C**) Representative images of migrated cells in transwell assays. (Scale bar = 100 μm.) (**D**) Migrated cells per field of view (scale bar = 100 μm) were analyzed (n=3). (**E**) Representative images of migrated areas at 0 h and 16 h in scratch assays. The yellow lines pointed out the edge of migrated cells. (Scale bar = 200 μm.) (**F**) Migrated areas per field of view (scale bar=200 μm) were analyzed (n=3). (**G**) Relative expression of fibrogenic-related genes (Col 1, Col3, and α-SMA) and adipogenic-related genes (PPARγ and C/EBPα) was detected by qRT-PCR (n=3). (H) The ratio of Col 3/Col 1 was analyzed (n=3). The significance was tested with an unpaired two-tailed Student's *t*-test. (**p*<0.05, ***p*<0.01, ****p*<0.01).

https://doi.org/10.2147/IJN.S411819 DovePress

related genes (PPARγ and C/EBPα) (Figure 5G), which might contribute to the reduction of scar formation. Besides, results also indicated that the ratio of Col 3/Col 1 was increased by ApoEVs-AT (Figure 5H), which was consistent with the experimental results in vivo (Figure 4F).

The cellular uptake of ApoEVs-AT by endothelial cells was also evaluated in this study. After culturing endothelial cells with Dio-labeled ApoEVs-AT for 4 h, ApoEVs-AT aggregation towards endothelial cells could be observed. After culturing for 8 h, ApoEVs-AT were detected inside endothelial cells (Figure 6A). The proliferation and migration of endothelial cells were also promoted by ApoEVs-AT (Figure 6B–D). Besides, tube formation assays showed that

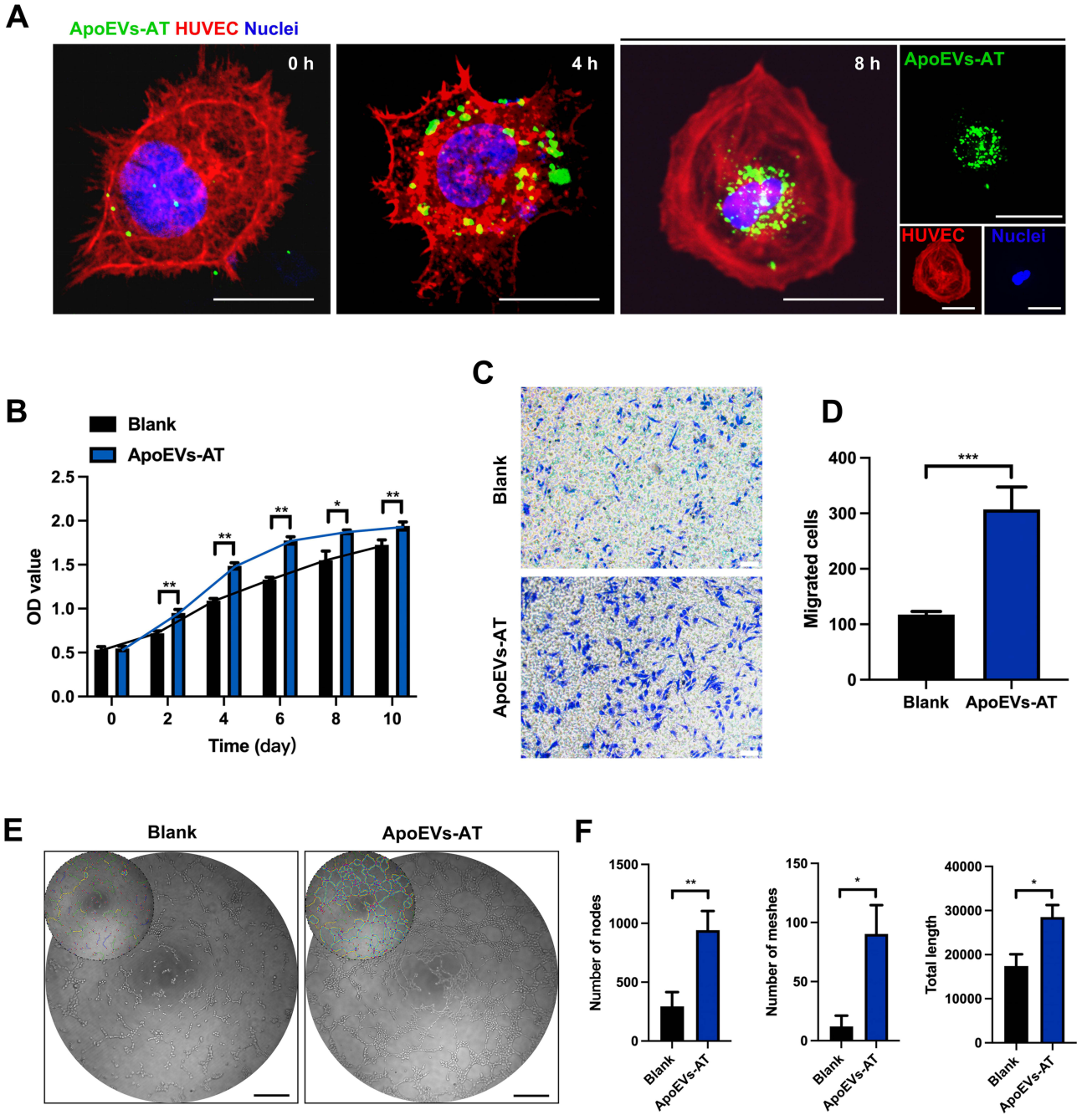

Figure 6 Behaviors of endothelial cells were regulated by ApoEVs-AT. (**A**) Uptake analysis of ApoEVs-AT by endothelial cells (Red: phalloidin-stained endothelial cells; Green: Dio-labeled ApoEVs-AT, blue: DAPI-stained nuclei. Scale bar = 40 μm.) (**B**) The proliferation of endothelial cells was measured by the CCK8 assays. (**C**) Representative images of migrated cells in transwell assays. (Scale bar = 100 μm.) (**D**) Migrated cells per field of view (scale bar = 100 μm) were analyzed (n=3). (**E**) Representative images of tube-like structure formation of endothelial cells. Images in the upper left area represented the results analyzed by ImageJ 1.53a software. (Scale bar = 500 μm.) (**F**) The number of nodes, number of meshes, and total length per field of view (scale bar = 500 μm) were analyzed (n=3). The significance was tested with an unpaired two-tailed Student's *t*-test. (**p*<0.05, ***p*<0.01, ****p*<0.01).

ApoEVs-AT significantly induced the angiogenesis of endothelial cells, based on the results that the number of nodes, the number of meshes, and total length were increased after pretreating endothelial cells with 50 μg/mL ApoEVs-AT (Figure 6E and F). Taken together, ApoEVs-AT promoted high-quality skin wound healing, which might be related to the regulation of the behavior of fibroblasts and endothelial cells.

Discussion

Due to the importance of dermal adipocytes in skin development and regeneration, transplantation of adipose tissue and its components was considered to be one of the most advanced therapies for skin repair. Many studies used adipose tissue,[23] nano fat,[24] adipose stromal cells (SVF),[25,26] ASCs,[27] and other cellular components to treat skin wounds and scars and showed therapeutic effects. However, cellular therapies have been restricted by factors such as necrosis, immune rejection, ethical issues, and tumor risk. Small extracellular vesicles, also known as exosomes, as the research hotspot of cell-free tissue engineering in the past years[28] and have been used for skin wound repair.[29–32] However, recent studies have shown that apoptosis occurred soon after cell transplantation,[7] so apoptotic extracellular vesicles (ApoEVs) were more likely to play a regulatory role than exosomes.

In this study, we first tried to isolate ApoEVs directly from adipose tissue. Tissue-derived ApoEVs were closer to the internal microenvironment under real conditions than single-cell-derived ApoEVs. So far, most of the studies have used staurosporine (STS) to induce apoptosis of MSCs.[14–17,19,33–35] STS, an antibiotic, was originally extracted from the bacterium *Streptomyces* in 1977[36] and reported to induce apoptosis by activating caspase 3 and preventing cells from being in the G1 or G2 phase of the cell cycle. Most studies treated MSCs with STS for no more than 16 hours. Considering the difference between tissues and cells, our study extended the culture time to 2 days. The results showed that after 2 days of culture, STS could successfully induce apoptosis of adipose tissue. To our surprise, the results of TEM and marker protein analysis indicated that ApoEVs-AT extracted from adipose tissue showed the characteristics of high purity. In other studies, Metronidazole[37] was used by Brock et al to induce the apoptosis of epithelial stem cells. H_2O_2 and starvation were also used by Zhang et al in their study.[14] Xin et al exposed stem cells to UVC light to induce apoptosis in UMSCs.[38] Le et al found that high hydrostatic pressure (HHP), one of the physical techniques, could effectively induce the apoptosis of MSCs.[39] This method contained no chemical reagent, so it was considered safe to manufacture therapeutic products simply. However, more studies were needed to investigate the characteristics and effectiveness in the disease treatment of ApoEVs induced by this method.

To further evaluate the therapeutic effect of ApoEVs-AT on full-thickness skin wounds, we made skin defects with a diameter of 2 cm, which could be considered as large defects in the wound healing model and was more prone to scar formation.[40] Since we did not mix ApoEVs-AT with any sustained-release materials, we injected ApoEVs-AT every 4 days to ensure the therapeutic effect. Compared with Qu et al's study in 2022 using PSCs- derived ApoEVs to promote skin wound healing,[18] we used tissue-derived ApoEVs to achieve the same effect and further improved the quality of wound healing. However, the delivery method needed to be further improved. No matter which injection method was used, it could only improve the function of ApoEVs-AT themself. An excellent drug delivery method, such as wrapping ApoEVs-AT in scaffolds, could not only reduce the iatrogenic trauma and pain caused by local injection, but also slowly release ApoEVs-AT, and improve the antibacterial and adhesive properties.[41–43] ApoEVs-AT showed sizes in the nanometer scales, so they were suitable for a variety of delivery methods. Therefore, in the future, we would combine ApoEVs-AT with a more efficient delivery method to maximize its value in the treatment of skin wounds.

Skin wound repair was a complex process; many kinds of cells were involved, including fibroblasts, endothelial cells, inflammatory cells, stem cells, etc.[1] Fibroblasts were the cells with the largest number and the most critical role. Although fibroblasts did not show the multi-directional differentiation potential of MSCs, they showed the ability to differentiate into fibroblasts or adipocytes.[44,45] Some studies also confirmed that PPARγ$^+$ or C/EBPα$^+$ preadipocytes were particularly critical for the regulation of skin development.[46,47] In this study, we treated fibroblasts with ApoEVs-AT for 20 days and the results showed ApoEVs-AT could promote the expression of PPARγ or C/EBPα, which might be related to the appearance of adipocytes in the ApoEVs-AT group in vivo. In normal skin, collagen 1 was the main type of collagen and was thick. Collagen 3 was relatively small. The presence of collagen 3 improved the softness and elasticity of the skin. Studies have shown that a higher relative proportion of collagen 3 meant better wound healing.[48] Our results were consistent with previous reports, which was reflected in

the increased ratio of Col 3: Col 1 in the ApoEV-AT group. The regulation of ApoEVs-AT on the behavior and differentiation direction of fibroblasts might be one of the key steps in ultimately reducing the area of scars.

In addition to the behavior of fibroblasts, the angiogenesis of endothelial cells also played a significant role in improving the rate and quality of skin wound healing.[49] Many cellular-based and non-cellular-based strategies have been used to enhance angiogenesis. In terms of using ApoEVs to promote angiogenesis, ApoEVs, isolated from human deciduous pulp stem cells, have been reported to recruit endogenous ECs and activate the angiogenic process in dental pulp regeneration.[19] In a myocardial infarction (MI) model, Liu et al found that after local transplantation, MSCs underwent apoptosis and released abundant ApoEVs, which were uptaken by ECs. Then, in these ECs, ApoEVs activated the function of lysosomes and increased the expression of TFEB, which was considered a master gene in the biogenesis of lysosomal and the process of autophagy. Finally, the increase of TFEB further enhanced the expression of autophagy-related genes in ECs and promoted angiogenesis activity.[34] In this study, our findings also indicated that adipose tissue-derived ApoEVs also showed the ability to promote the proliferation, migration, and angiogenesis of ECs, which largely contributed to improving skin wound healing and scar remodeling.

Despite these results confirming the therapeutical potential of ApoEVs-AT, there are some limitations. For example, the components of ApoEVs-AT (proteins, nucleic acids, lipids) need further testing. Which components of ApoEVs-AT play the key role in the repair of skin wounds is unclear. The molecular mechanisms by which ApoEVs-AT regulate various cells require further exploration. Only by clarifying the issues related to the mechanism could sufficient theoretical support be provided for the effectiveness and safety of clinical transformation.

Conclusion

In conclusion, we, for the first study, isolated ApoEVs-AT from adipose tissue and confirmed that it showed encouraging effectiveness in skin wound repair. Besides, we also indicated that the ability of ApoEVs-AT to induce high-quality full-thickness skin wounds might be related to the regulation of the behavior of fibroblasts and endothelial cells. Considering the abundant sources, high yield, and guaranteed effectiveness, ApoEVs-AT appeared to be a potential raw material for further application.

Author Contributions

All authors made a significant contribution to the work reported, whether that is in the conception, study design, execution, acquisition of data, analysis and interpretation, or in all these areas; took part in drafting, revising or critically reviewing the article; gave final approval of the version to be published; have agreed on the journal to which the article has been submitted; and agree to be accountable for all aspects of the work.

Funding

This study was funded by Shenzhen Science and Technology Program (JCYJ20220530165014032), China Postdoctoral Science Foundation (2022M722257), and Construction Funds of Key Medical Disciplines in Longhua District, Shenzhen (MKD202007090212).

Disclosure

The authors report no conflicts of interest in this work.

References

1. Rodrigues M, Kosaric N, Bonham C, Gurtner G. Wound healing: a cellular perspective. *Physiol Rev*. 2019;99(1):665–706. doi:10.1152/physrev.00067.2017
2. Nosrati H, Khodaei M, Alizadeh Z, Banitalebi-Dehkordi M. Cationic, anionic and neutral polysaccharides for skin tissue engineering and wound healing applications. *Int J Biol Macromol*. 2021;192:298–322. doi:10.1016/j.ijbiomac.2021.10.013
3. Dong J, Wu B, Tian W. How to maximize the therapeutic effect of exosomes on skin wounds in diabetes mellitus: review and discussion. *Front Endocrinol*. 2023;14:1146991. doi:10.3389/fendo.2023.1146991
4. Zhang Z, Shao M, Hepler C, et al. Dermal adipose tissue has high plasticity and undergoes reversible dedifferentiation in mice. *J Clin Invest*. 2019;129(12):5327–5342. doi:10.1172/JCI130239
5. Liu S, Jiang L, Li H, et al. Mesenchymal stem cells prevent hypertrophic scar formation via inflammatory regulation when undergoing apoptosis. *J Invest Dermatol*. 2014;134(10):2648–2657. doi:10.1038/jid.2014.169

6. Galleu A, Riffo-Vasquez Y, Trento C, et al. Apoptosis in mesenchymal stromal cells induces in vivo recipient-mediated immunomodulation. *Sci Transl Med*. 2017;9(416). doi:10.1126/scitranslmed.aam7828
7. Fu Y, Sui B, Xiang L, et al. Emerging understanding of apoptosis in mediating mesenchymal stem cell therapy. *Cell Death Dis*. 2021;12(6):596. doi:10.1038/s41419-021-03883-6
8. Kerr JF, Wyllie AH, Currie AR. Apoptosis: a basic biological phenomenon with wide-ranging implications in tissue kinetics. *Br J Cancer*. 1972;26 (4):239–257. doi:10.1038/bjc.1972.33
9. Elmore S. Apoptosis: a review of programmed cell death. *Toxicol Pathol*. 2007;35(4):495–516. doi:10.1080/01926230701320337
10. Atkin-Smith GK, Tixeira R, Paone S, et al. A novel mechanism of generating extracellular vesicles during apoptosis via a beads-on-a-string membrane structure. *Nat Commun*. 2015;6:7439. doi:10.1038/ncomms8439
11. Ye Q, Xu H, Liu S, et al. Apoptotic extracellular vesicles alleviate Pg-LPS induced inflammation of macrophages via AMPK/SIRT1/NF-κB pathway and inhibit adjacent osteoclast formation. *J Periodontol*. 2022;93:1738–1751. doi:10.1002/JPER.21-0657
12. Li M, Xing X, Huang H, et al. BMSC-Derived ApoEVs promote craniofacial bone repair via ROS/JNK signaling. *J Dent Res*. 2022;101 (6):714–723. doi:10.1177/00220345211068338
13. Ou Q, Tan L, Shao Y, et al. Electrostatic charge-mediated apoptotic vesicle biodistribution attenuates sepsis by switching neutrophil NETosis to apoptosis. *Small*. 2022;18(20):e2200306. doi:10.1002/smll.202200306
14. Zhang X, Tang J, Kou X, et al. Proteomic analysis of MSC-derived apoptotic vesicles identifies Fas inheritance to ameliorate haemophilia a via activating platelet functions. *J Extracelr Ves*. 2022;11(7). doi:10.1002/jev2.12240
15. Ma L, Chen C, Liu D, et al. Apoptotic extracellular vesicles are metabolized regulators nurturing the skin and hair. *Bio Mat*. 2023;19:626–641. doi:10.1016/j.bioactmat.2022.04.022
16. Wang J, Cao Z, Wang P, et al. Apoptotic extracellular vesicles ameliorate multiple myeloma by restoring fas-mediated apoptosis. *ACS nano*. 2021;15(9):14360–14372. doi:10.1021/acsnano.1c03517
17. Zheng C, Sui B, Zhang X, et al. Apoptotic vesicles restore liver macrophage homeostasis to counteract type 2 diabetes. *J Extracel Ves*. 2021;10(7): e12109. doi:10.1002/jev2.12109
18. Qu Y, He Y, Meng B, et al. Apoptotic vesicles inherit SOX2 from pluripotent stem cells to accelerate wound healing by energizing mesenchymal stem cells. *Acta Biomater*. 2022;149:258–272. doi:10.1016/j.actbio.2022.07.009
19. Li Z, Wu M, Liu S, et al. Apoptotic vesicles activate autophagy in recipient cells to induce angiogenesis and dental pulp regeneration. *Mol Ther*. 2022;30:3193–3208. doi:10.1016/j.ymthe.2022.05.006
20. Rahimipour S, Salahinejad E, Sharifi E, Nosrati H, Tayebi L. Structure, wettability, corrosion and biocompatibility of nitinol treated by alkaline hydrothermal and hydrophobic functionalization for cardiovascular applications. *Appl Surf Sci*. 2020;506:144657. doi:10.1016/j.apsusc.2019.144657
21. Merrick D, Seale P. Skinny fat cells stimulate wound healing. *Cell Stem Cell*. 2020;26(6):801–803. doi:10.1016/j.stem.2020.04.021
22. Guerrero-Juarez C, Plikus M. Emerging nonmetabolic functions of skin fat. *Nat Rev Endocrinol*. 2018;14(3):163–173. doi:10.1038/nrendo.2017.162
23. Fredman R, Katz AJ, Hultman CS. Fat grafting for burn, traumatic, and surgical scars. *Clin Plast Surg*. 2017;44(4):781–791. doi:10.1016/j.cps.2017.05.009
24. Jan SN, Bashir MM, Khan FA, et al. Unfiltered nanofat injections rejuvenate postburn scars of face. *Ann Plast Surg*. 2019;82(1):28–33. doi:10.1097/SAP.0000000000001631
25. Giudice G, Filoni A, Maggio G, et al. Use of the stromal vascular fraction in intermediate-deep acute burns: a case with its own control. *J Burn Care Res*. 2018;39(5):846–849. doi:10.1093/jbcr/irx017
26. Karakol P, Bozkurt M, Gelbal C, Tuglu MI. Efficacy of stromal vascular fraction and enzyme-free mechanical isolation therapy in experimental full thickness burn wounds. *J Plast Surg Hand Surg*. 2021;2021:1–17.
27. Muhammad G, Xu J, Bulte JWM, Jablonska A, Walczak P, Janowski M. Transplanted adipose-derived stem cells can be short-lived yet accelerate healing of acid-burn skin wounds: a multimodal imaging study. *Sci Rep*. 2017;7(1):4644. doi:10.1038/s41598-017-04484-0
28. Dong J, Wu B, Tian W. Adipose tissue-derived small extracellular vesicles modulate macrophages to improve the homing of adipocyte precursors and endothelial cells in adipose tissue regeneration. *Front Cell Dev Biol*. 2022;10:1075233. doi:10.3389/fcell.2022.1075233
29. Li Y, Zhang J, Shi J, et al. Exosomes derived from human adipose mesenchymal stem cells attenuate hypertrophic scar fibrosis by miR-192-5p/IL-17RA/Smad axis. *Stem Cell Res Ther*. 2021;12(1):221. doi:10.1186/s13287-021-02290-0
30. Zhang W, Bai X, Zhao B, et al. Cell-free therapy based on adipose tissue stem cell-derived exosomes promotes wound healing via the PI3K/Akt signaling pathway. *Exp Cell Res*. 2018;370(2):333–342. doi:10.1016/j.yexcr.2018.06.035
31. Qian L, Pi L, Fang B, Meng X. Adipose mesenchymal stem cell-derived exosomes accelerate skin wound healing via the lncRNA H19/miR-19b/SOX9 axis. *Lab Invest*. 2021;101(9):1254–1266.
32. Dong J, Wu Y, Zhang Y, Yu M, Tian W. Comparison of the therapeutic effect of allogeneic and xenogeneic small extracellular vesicles in soft tissue repair. *Int J Nanomedicine*. 2020;15:6975–6991. doi:10.2147/IJN.S269069
33. Liu D, Kou X, Chen C, et al. Circulating apoptotic bodies maintain mesenchymal stem cell homeostasis and ameliorate osteopenia via transferring multiple cellular factors. *Cell Res*. 2018;28(9):918–933. doi:10.1038/s41422-018-0070-2
34. Liu H, Liu S, Qiu X, et al. Donor MSCs release apoptotic bodies to improve myocardial infarction via autophagy regulation in recipient cells. *Autophagy*. 2020;16(12):2140–2155.
35. Liu J, Qiu X, Lv Y, et al. Apoptotic bodies derived from mesenchymal stem cells promote cutaneous wound healing via regulating the functions of macrophages. *Stem Cell Res Ther*. 2020;11(1):507. doi:10.1186/s13287-020-02014-w
36. Omura S, Iwai Y, Hirano A, et al. A new alkaloid AM-2282 OF Streptomyces origin. Taxonomy, fermentation, isolation and preliminary characterization. *J Antibiot*. 1977;30(4):275–282. doi:10.7164/antibiotics.30.275
37. Brock CK, Wallin ST, Ruiz OE, et al. Stem cell proliferation is induced by apoptotic bodies from dying cells during epithelial tissue maintenance. *Nat Commun*. 2019;10(1):1044. doi:10.1038/s41467-019-09010-6
38. Xin L, Wei C, Tong X, et al. In situ delivery of apoptotic bodies derived from mesenchymal stem cells via a hyaluronic acid hydrogel: a therapy for intrauterine adhesions. *Bio Mat*. 2022;12:107–119. doi:10.1016/j.bioactmat.2021.10.025
39. Le TM, Morimoto N, Ly NT, et al. Ex vivo induction of apoptotic mesenchymal stem cell by high hydrostatic pressure. *Stem Cell Rev Rep*. 2021;17 (2):662–672. doi:10.1007/s12015-020-10071-0

40. Zhou Y, Zhang XL, Lu ST, et al. Human adipose-derived mesenchymal stem cells-derived exosomes encapsulated in pluronic F127 hydrogel promote wound healing and regeneration. *Stem Cell Res Ther*. 2022;13(1):407.
41. Jiang T, Liu S, Wu Z, et al. ADSC-exo@MMP-PEG smart hydrogel promotes diabetic wound healing by optimizing cellular functions and relieving oxidative stress. *Materials Today Bio*. 2022;16:100365. doi:10.1016/j.mtbio.2022.100365
42. Wang C, Liang C, Wang R, et al. The fabrication of a highly efficient self-healing hydrogel from natural biopolymers loaded with exosomes for the synergistic promotion of severe wound healing. *Biomaterials sci*. 2019;8(1):313–324. doi:10.1039/C9BM01207A
43. Geng X, Qi Y, Liu X, Shi Y, Li H, Zhao L. A multifunctional antibacterial and self-healing hydrogel laden with bone marrow mesenchymal stem cell-derived exosomes for accelerating diabetic wound healing. *Bio Adv*. 2022;133:112613. doi:10.1016/j.msec.2021.112613
44. Driskell R, Lichtenberger B, Hoste E, et al. Distinct fibroblast lineages determine dermal architecture in skin development and repair. *Nature*. 2013;504(7479):277–281. doi:10.1038/nature12783
45. Plikus M, Guerrero-Juarez C, Ito M, et al. Regeneration of fat cells from myofibroblasts during wound healing. *Science*. 2017;355(6326):748–752. doi:10.1126/science.aai8792
46. Wojciechowicz K, Markiewicz E, Jahoda C. C/EBPalpha identifies differentiating preadipocytes around hair follicles in foetal and neonatal rat and mouse skin. *Exp Dermatol*. 2008;17(8):675–680. doi:10.1111/j.1600-0625.2007.00689.x
47. Wang F, Mullican S, DiSpirito J, Peed L, Lazar M. Lipoatrophy and severe metabolic disturbance in mice with fat-specific deletion of PPARγ. *Proc Natl Acad Sci U S A*. 2013;110(46):18656–18661. doi:10.1073/pnas.1314863110
48. Dalirfardouei R, Jamialahmadi K, Jafarian AH, Mahdipour E. Promising effects of exosomes isolated from menstrual blood-derived mesenchymal stem cell on wound-healing process in diabetic mouse model. *J Tissue Eng Regen Med*. 2019;13(4):555–568. doi:10.1002/term.2799
49. Nosrati H, Aramideh Khouy R, Nosrati A, et al. Nanocomposite scaffolds for accelerating chronic wound healing by enhancing angiogenesis. *J Nanobiotechnology*. 2021;19(1):1. doi:10.1186/s12951-020-00755-7